AIAA AVIATION Forum
5-9 June 2017, Denver, Colorado
33rd AIAA Aerodynamic Measurement Technology and Ground Testing Conference

Krypton Tagging Velocimetry in the Stevens Shock Tube

M. A. Mustafa* N. J. Parziale†
Stevens Institute of Technology, Hoboken, NJ 07030, USA

Krypton Tagging Velocimetry (KTV) is implemented in the flow immediately following the incident shock wave in the Stevens Shock Tube. This is motivated by the long-term goal of using KTV to measure velocity in large-scale impulse facilities. Two example cases are presented in 99% N_2/1% Kr at incident shock Mach numbers of 2.86 and 2.94. The velocities as measured by KTV are, in general, higher than those calculated from the shock-speed measurements. The discrepancy is most likely due to the misalignment of splitter plate installed in the shock tube (an expansion fan likely accelerated the flow). A new excitation scheme for KTV is used that results in a higher SNR as compared to previous work. A justification of the alternate scheme is presented via a three energy level model. An overview of the shock tube is given, and a model predicting the non-equilibrium thermodynamic state of the gas immediately following the incident shock is presented.

Nomenclature

N = Population of energy state, (#)
T = Translational and rotational temperature, (K)
Q = Quenching rate of excited/re-excited state, (s^{-1})
b = Rate of stimulated emission, (s^{-1})
b' = Rate of stimulated absorption, (s^{-1})
q = Specific quenching rate for excited state, (s^{-1})
A = Einstein A coefficient for transition, (s^{-1})
X = Mole fraction, (-)
P = Pressure, (torr)
a = Sound speed, (m/s)
u = Velocity, (m/s)
ρ = Density, (kg/m^3)
γ = Ratio of specific heats, (-)
M = Mach number, (-)
t = Time, (s)
t_0 = Time at end of read pulse (s)
R = Specific gas constant, (J/(kg K))
e_v = Internal energy due to vibration , (J/kg)
e_v^{eq} = Equilibrium vibrational energy, (J/kg)
τ = Vibrational-relaxation time, (s)
h = Plank's constant, (m^2kg/s)
k = Boltzmann's constant, ($m^2kg/(s^2\ K)$)
x = Distance behind shock, (m)
f = Frequency of emitted light, (Hz)
Ω = Collection solid angle, (sr)
V = Emitting volume, (m^3)

*Graduate Student, Mechanical Engineering, Castle Point on Hudson, Hoboken, New Jersey, 07030.
†Assistant Professor, Mechanical Engineering, Castle Point on Hudson, Hoboken, New Jersey, 07030, AIAA Member.

Subscript

m = Metastable state $5s[3/2]_2^o$
r = Resonance state $5s[3/2]_1^o$
e = Original excited/re-excited state $5p[3/2]_2$
e' = Alternative re-excited state $5p[3/2]_1$
1 = Ahead of shock (driven section)
2 = Behind shock, relative to shock
4 = Driver section
s = Shock wave
$2L$ = Behind shock, lab frame
$2LF$ = Behind shock, lab frame, frozen property
$2F$ = Behind shock, frozen property
ji = Transition between energy states j and i
jm = Transition between arbitrary excited/re-excited state j and metastable state $5s[3/2]_2^o$
jr = Transition between arbitrary state excited/re-excited j and resonance state $5s[3/2]_1^o$
em = Transition between states $5p[3/2]_2$ and $5s[3/2]_2^o$
er = Transition between states $5p[3/2]_2$ and $5s[3/2]_1^o$
$e'm$ = Transition between states $5p[3/2]_1$ and $5s[3/2]_2^o$
$e'r$ = Transition between states $5p[3/2]_1$ and $5s[3/2]_1^o$

I. Introduction

Non-intrusive techniques are becoming increasingly popular for making measurements in high-speed flows. A laser pulse is often used to tag a region in the flow so that its evolution in time and space can be observed because the tagged region is in some fashion different from its surroundings. This data can then be used to determine flow properties such as the velocity.

The Laser Doppler Velocimetry (LDV) technique utilizes the Doppler shift effect to measure particle velocity. An incident laser beam is directed into the flow at tracer particles. The beam is then scattered by the particles and received by a detector. The difference in frequency of the incident and scattered beams can be processed to yield the velocity of the particle.[1] However, one significant disadvantage of this technique is that it can only make point measurements in the flow. An additional drawback is that particle seeding is required.

Particle Image Velocimetry (PIV) is another laser-based velocimetry technique. The working principle is that tracer particles are imaged in the flow and their displacement over a period of time is related to the flow velocity. As far as application in impulse facilities, PIV was applied to the flow inside a shock tunnel by Haertig et al.,[2] where velocities of up to 2 km/s were measured with an accuracy of a few percent when compared to the theoretical values.

PIV measurements rely on the assumption that the tracer particles travel with the same velocity as the flow. An important factor in PIV is the dynamics of the injected particle relative to the flow. The parameters of interest are the response time and the Stokes number. If these quantities are appropriate, the particle follows the streamlines of the flow. In the supersonic regime, this is found to not be an issue by Wagner et al.,[3] where the response time was determined to be 5.9 µs at relatively high densities. However, at low densities, the dynamics of the particles can compromise PIV measurement accuracy, particularly at finer scales. Loth[4] found that at low densities the Knudsen number of a particle can become large, which results in a slip condition at the surface. This means that the particle can lag behind the local fluid velocity resulting in uncertainty. Timing and seeding issues associated with PIV are technical in nature and may be addressed in certain situations. However, reduced particle response is a fundamental limitation that may not be overcome when attempting to apply PIV in certain flows.

An alternative laser velocimetry technique, tagging velocimetry,[5] will be the focus of this paper. Tagging velocimetry is typically performed in gases by tracking the fluorescence of a native, seeded, or synthesized gas. In contrast to the limitations of implementing PIV techniques in high-speed facilities, the implementation of tagging velocimetry is not limited by timing issues associated with tracer injection[2] or reduced particle response at Knudsen and Reynolds numbers[4] typical of high-speed wind tunnels. Noted methods of tagging

velocimetry include the VENOM,[6–10] APART,[11–13] RELIEF,[14–18] FLEET,[19,20] STARFLEET,[21] PLEET,[22] argon,[23] iodine,[24,25] sodium,[26] acetone,[27–29] and the hydroxyl group techniques,[30–32] among others.[33–37]

This paper presents how Krypton Tagging Velocimetry (KTV) was applied to the flow behind the incident shock in the Stevens Shock Tube. The goal was to assess the viability of the KTV technique for use in large-scale impulse facilities. We present details on the experimental setup, the excitation scheme, and the results.

II. Stevens Shock Tube

To assess the viability of the KTV technique in impulse facilities, a shock tube was designed and constructed at the Stevens Institute of Technology. The goal is to create static thermodynamic conditions behind the incident shock wave that are similar to those in the freestream in larger facilities, albeit at lower velocity in the Stevens Shock Tube. This is to demonstrate that KTV may be implemented at new conditions, as previous work has been performed in cold flows. The shock tube schematic is shown in Fig. 1. The end section is part of the driven section but is made separate to allow for the installation and maintenance of the four optical access ports, shown in Fig. 2. The diaphragm for the current experiments is 0.005" thick aluminum. There is a piercing mechanism that ruptures the diaphragm, shown in Fig. 2. It is comprised of a solenoid, a rod and a blade. Three pressure sensors are placed on the tube (P1, P2 and P3) are used to find the shock speed. The port marked "intake" in Fig. 1 is where the gas mixtures are seeded into the tube.

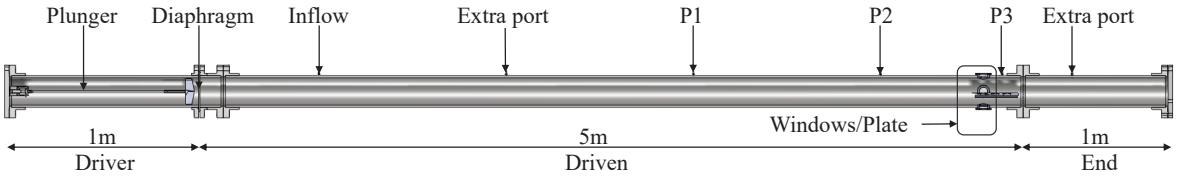

Figure 1: Schematic of the Stevens Shock Tube. The pipe is 6 inch nominal diameter, schedule 80.

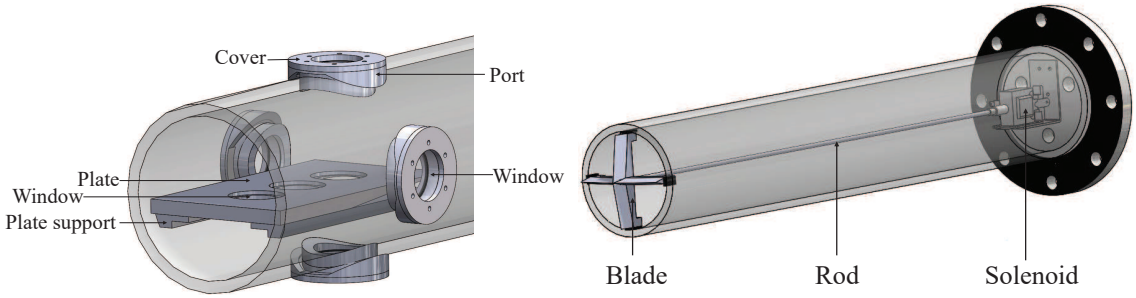

Figure 2: **Left:** Window ports and plate for laser diagnostics. **Right:** Diaphragm rupturing mechanism.

For a calorically-perfect gas, the expected Mach number of the shock wave as a function of the pressure ratio and driver/driver gases in a shock tube is,

$$\frac{P_4}{P_1} = \frac{2\gamma_1 M_s^2 - (\gamma_1 - 1)}{\gamma_1 + 1}\left\{1 - \frac{\gamma_4 - 1}{\gamma_1 + 1}\frac{a_1}{a_4}\left(M_s - \frac{1}{M_s}\right)\right\}^{\frac{-2\gamma_4}{\gamma_4 - 1}}. \tag{1}$$

Equation (1) is plotted in Fig. 3 for three different values of a_4/a_1, corresponding to air as the driven gas and air, argon and helium as the driver gas, respectively. Using air as the driver and driven gas, several runs were conducted at several pressure ratios (with the driver at atmospheric pressure) with the goal of shaking down the Stevens Shock Tube. These results appear along the $a_4/a_1 = 1$ line in Fig. 3, and show good agreement with uncertainty predicted as per Moffat,[38]

$$\delta R = \sqrt{(\frac{\partial R}{\partial x_1}\delta x_1)^2 + (\frac{\partial R}{\partial x_2}\delta x_2)^2 + ...(\frac{\partial R}{\partial x_n}\delta x_n)^2}. \tag{2}$$

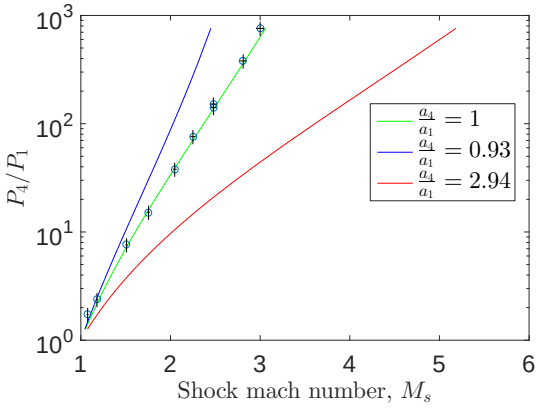

Figure 3: Pressue ratio vs shock Mach number for different driver gases.

From the experimental shock-speed data, we conclude that there is a sufficient level of control of conditions in the shock tube to explore KTV viability over the parameter space of interest. Fig. 4 shows plots of the pressure readings for incident shock Mach numbers of 1.06 and 3.00. In these cases, P_1 was approximately 440 torr and 1 torr, respectively. Fig. 4 shows also shows the useful test time of ≈1 ms when the measurements will be made with KTV at the $M_s = 3.00$ case which creates static thermodynamic conditions that are similar to that in a large-scale impulse facility.

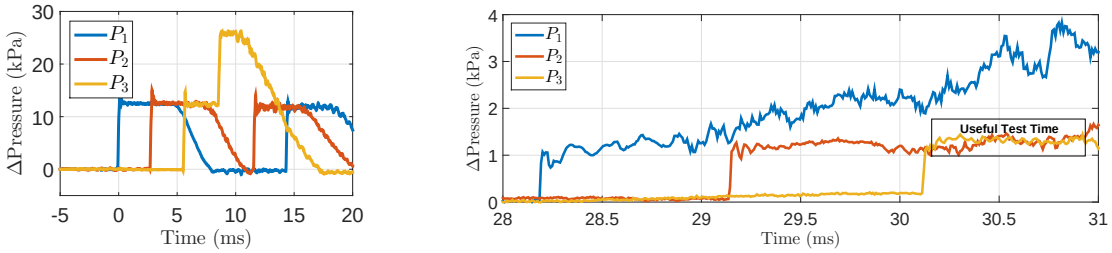

Figure 4: Pressure data. **Left:** Shock Mach number of 1.06. **Right:** Shock Mach number of 3.00.

III. Conditions Behind Shock Wave in N_2

To predict the conditions behind the shock wave, a one-dimensional, shock-fixed, steady-state, thermal non-equilibrium model was used. N_2 dissociation was not considered. In the model, the working fluid was assumed to be 100% N_2; the 0.01 mole fraction of Kr was neglected. The following governing equations of mass, momentum, and energy, were used following Anderson[39] as

$$\rho_2 \frac{du_2}{dx} + u_2 \frac{d\rho_2}{dx} = 0, \tag{3}$$

$$\rho_2 u_2 \frac{du_2}{dx} + R\rho_2 \frac{dT_2}{dx} + RT_2 \frac{d\rho_2}{dx} = 0, \tag{4}$$

and

$$3.5R \frac{dT_2}{dx} + u_2 \frac{du_2}{dx} + \frac{de_v}{dx} = 0. \tag{5}$$

Here, u_2 is the velocity (in the shock-fixed frame), ρ_2 is the density, and T_2 is the transnational and rotational temperature in region 2 (behind the shock). R is the specific gas constant, and e_v is the internal energy due to vibration. In Eqs. (3-5), the ideal gas law was used to remove the pressure as a variable. Again, following Anderson,[39] the change in vibrational energy was modeled as,

$$u_2 \frac{de_v}{dx} = \frac{e_v^{eq} - e_v}{\tau}. \tag{6}$$

Here, e_v^{eq} is the equilibrium vibrational energy, which can be written as

$$e_v^{eq} = \frac{hv}{kT_2\left(\exp\left(\frac{hv}{kT_2}\right)-1\right)}RT_2. \tag{7}$$

Here, h is Plank's constant, k is Boltzmann's constant, and ν is the characteristic vibrational frequency. The vibrational-relaxation time, τ, was modeled as in Millikan and White[40] as

$$\tau P_2 = \exp\left[A(T^{-\frac{1}{3}} - 0.015\mu^{0.25}) - 18.42\right]. \tag{8}$$

Here, P_2 is the pressure after the shock, $A = 0.00116\mu^{0.5}(\frac{hv}{k})^{\frac{4}{3}}$ and $\mu = \frac{MW_{gas}}{2}$. MW_{gas} is the molecular weight of the gas. The velocity in the lab frame, u_{2L}, is given by

$$u_{2L} = M_s\sqrt{\gamma RT_1} - u_2, \tag{9}$$

and is the quantity that will be compared to KTV measurements. Here, T_1 is the temperature in region 1 (driven section) of the shock tube. The equations above represent a system of differential equations. To aid in their numerical solution, Eqs. (3-6) are re-written explicitly here as

$$\frac{du_2}{dx} = \frac{e_v - e_v^{eq}}{\tau(3.5RT_2 - 2.5u_2^2)}, \tag{10}$$

$$\frac{d\rho_2}{dx} = \frac{\rho_2(e_v^{eq} - e_v)}{\tau(3.5RT_2u_2 - 2.5u_2^3)}, \tag{11}$$

$$\frac{dT_2}{dx} = \frac{(RT_2 - u_2^2)(e_v^{eq} - e_v)}{\tau Ru_2(3.5RT_2 - 2.5u_2^2)}, \tag{12}$$

and

$$\frac{de_v}{dx} = \frac{1}{u_2}\frac{e_v^{eq} - e_v}{\tau}. \tag{13}$$

The initial conditions are calculated by the calorically-perfect normal-shock relations. Fig. 5 shows the solution of the equations for a shock speed of 1030 m/s, $P_1 = 0.95$ torr, and T_1 was 300 K. These are conditions from an example experiment where the highest shock speed was measured. The highest shock speed case is of interest as a bounding case because it represents an instance for vibrational non-equilibrium

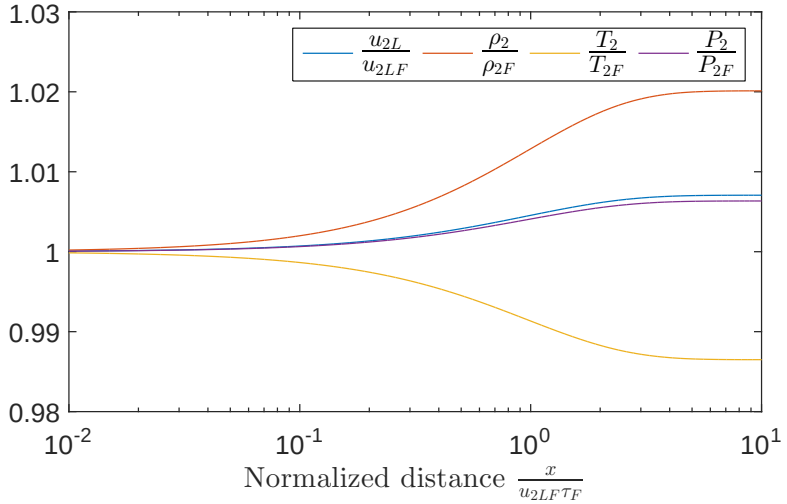

Figure 5: Normalized conditions behind shock wave in N_2 accounting for vibrational non-equilibrium.

to alter the conditions after the incident shock. In Fig. 5, the flow properties have been normalized with respect to their initial conditions, denoted by the subscript F, the frozen flow values. The distance after the shock wave, x, was normalized with respect to a characteristic distance, $u_{2LF}\tau_F$, where τ_F is a characteristic time scale and u_{2LF} (frozen velocity in region 2 in the lab frame) is a characteristic velocity scale. As Fig. 5 shows, the properties do not change significantly behind the incident shock and the flow can be analyzed as calorically perfect. Should the incident shock speed be increased further, this assumption will have to be reassessed. In addition, as a check on the calculations, Cantera[41] and the Shock and Detonation Toolbox[42] were used to compute the conditions post shock. Cantera assumes local thermodynamic equilibrium, and the present calculations at equilibrium match the Cantera results to less than 0.5%, bringing confidence to that calculations.

IV. Krypton Tagging Velocimetry (KTV) Setup

Krypton Tagging Velocimetry (KTV), relative to other tagging velocimetry techniques, relies on a chemically inert tracer. This property may enable KTV to broaden the utility of tagging velocimetry because the technique can be applied in gas flows where the chemical composition is difficult to prescribe or predict. The use of a metastable noble gas as a tagging velocimetry tracer was first suggested by Mills et al.[43] and Balla and Everheart.[44] KTV was first demonstrated by Parziale et al.[45,46] to measure the velocity along the center-line of an underexpanded jet of N_2/Kr mixtures. In that work, pulsed tunable lasers were used to induce fluorescence of Kr atoms that were seeded into the flow for the purposes of displacement tracking. Following that work, Zahradka et al.[47,48] used KTV to make measurements of the mean and fluctuating turbulent boundary-layer profiles in a Mach 2.7 flow. Recently, Mustafa et al.[49] used KTV to measure seven simultaneous profiles of streamwise velocity and velocity fluctuations in the incoming boundary layer and immediately upstream of a 24-degree compression corner in a $M_\infty = 2.8$, $\mathrm{Re}_\Theta = 1750$, 99% N_2/1% Kr shock-wave/turbulent boundary-layer interaction.

The setup of the laser system is similar to that found in Zahradka et al.[47,48] It consists of four parts, the write laser, the read laser, the camera and the controls. The controls presented a new challenge in the form of the timing of the lasers and the camera with the passage of the shock while keeping the laser system at operating temperature. As Fig. 6 shows, the lasers are controlled by the SRS DG 645 pulse generator. This pulse generator is triggered by the combined signal from the SRS DS 345 function generator and the SRS DG 535 pulse generator. The function generator outputs a 10 Hz pulse, and the SRS DG 535 pulse generator outputs a pulse only when the amplified signal of P2 reaches a certain value. This happens when the shock passes over P2 in the shock tube. Once the amplified P2 signal crosses the threshold, the SRS DG 535 outputs a pulse that triggers the SRS DG 645, which in turn triggers the lasers after a set delay. This allows for making measurements a set time after the shock has passed over while keeping the laser system at operating temperature. The BNC 577 pulse generator is used to activate the solenoid and rupture the diaphragm. It is triggered by the SRS DG 645 with a set delay to ensure that the write laser pulse is roughly 90-100 ms after the previous laser pulse.

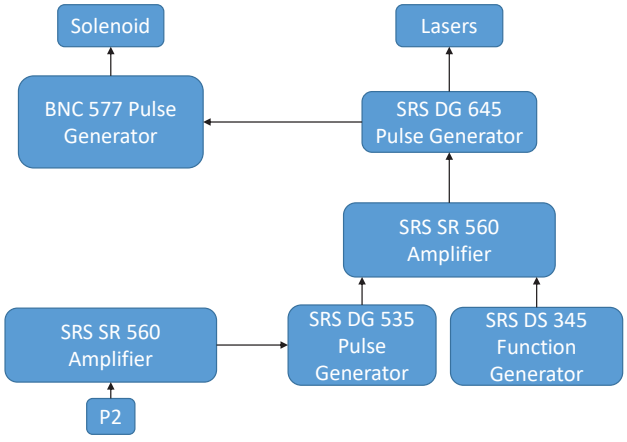

Figure 6: Schematic of timing/wiring for KTV in Stevens Shock Tube.

V. Alternative Re-Excitation Scheme

It is desirable to create the brightest fluorescence possible to capture the highest quality images when using a tagging velocimetry technique. To this end, we propose an alternative re-excitation scheme that results in approximately twice as much fluorescence as the original one used by Zahradka et al.[47,48] In this proposed excitation scheme, the read laser pulse will be used to excite the $5s[3/2]_2^o$ to $5p[3/2]_1$ transition, as opposed to the $5s[3/2]_2^o$ to $5p[3/2]_2$ transition. The fluorescence that will be imaged is from the $5p[3/2]_1 \rightarrow 5s[3/2]_1^o$ transition on the read step. A schematic is shown in Fig. 7, where A, B, C, and D represent the relevant transitions.

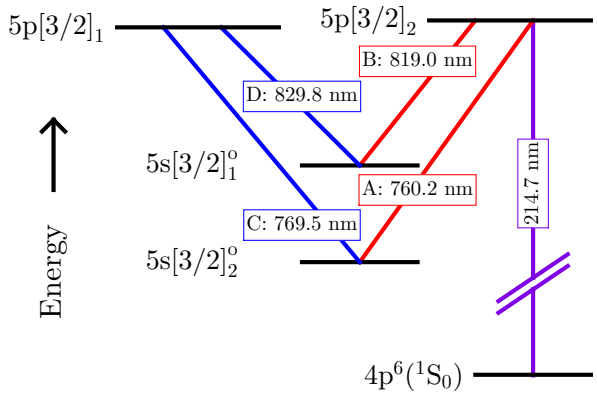

Figure 7: Energy diagram for alternate re-excitation scheme. Racah nl[K]$_J$ notation, A, B, C and D represent the transitions between the states.

The alternative scheme is performed in the following three steps. The third step is what differs from the original scheme.

1. Seed a base flow with krypton globally.
2. Photosynthesize metastable krypton atoms with a pulsed tunable laser to form the tagged tracer: two-photon excitation of $4p^6(^1S_0) \rightarrow 5p[3/2]_2$ (214.7 nm) and rapid decay to resonance state $5p[3/2]_2 \rightarrow 5s[3/2]_1^o$ (819.0 nm, transition B) and metastable state $5p[3/2]_2 \rightarrow 5s[3/2]_2^o$ (760.2 nm, transition A). We estimate that the creation of the metastable atoms which comprise the "write line" takes approximately 50 ns.[50] The position of the write line is marked by the fluorescence from the $5p[3/2]_2 \rightarrow 5s[3/2]_1^o$ transitions (819.0 nm, transition B), and is recorded with a camera positioned normal to the flow.
3. Record the displacement of the tagged metastable krypton by imaging the laser induced fluorescence (LIF) that is produced with an additional pulsed tunable laser: excite $5p[3/2]_1$ level by $5s[3/2]_2^o \rightarrow 5p[3/2]_1$ transitions with laser sheet (769.5 nm, transition C) and read spontaneous emission of $5p[3/2]_1 \rightarrow 5s[3/2]_1^o$ (829.8 nm, transition D) transitions with a camera positioned normal to the flow.

VI. KTV Model

To justify the alternative strategy outlined in the previous section, a three energy level model is presented here (Fig. 8). State r is the resonance state $5s[3/2]_1^o$ whose population is given by N_r, state m is the metastable state $5s[3/2]_2^o$ whose population is given by N_m and state j is the excited state whose population is given by N_j. The variable j may refer to the $5p[3/2]_1$ or $5p[3/2]_2$ energy level. The goal of the model is to determine $N_r(t)$, $N_m(t)$, and $N_j(t)$. This will allow for the calculation of the parameter $N_j A_{jr}(t)$, which is proportional to the SNR. Eckbreth[51] states the signal of a fluorescence technique, F, can be calculated as

$$F = hfN_jA_{jr}\Omega V/(4\pi) \tag{14}$$

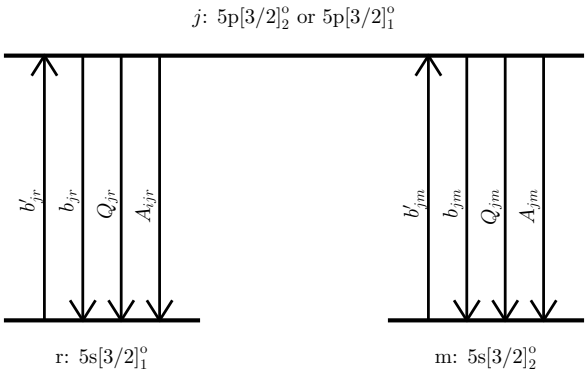

Figure 8: Three level model of energy states of krypton. We denote the excited state as j, the resonance state as r, and the metastable state as m.

where h is Planck's constant, f is the frequency of emitted light, N is the population, A is the Einstein coefficient, Ω is the collection solid angle, and V is the emitting volume.

The model will be broken into two parts: 1) when the read-laser pulse is on; and 2) when the read-laser pulse is off (which is when the fluorescence is recorded by the camera). The governing equations for the populations are the same for both parts of the model, except the excitation-rate constant is set to zero when the laser is off. For simplicity, we will assume that all else but the excitation strategy is the same (A vs. C. in Fig. 7). Following Fig. 8, we can write differential equations that govern the populations as

$$\frac{dN_r}{dt} = -N_r b'_{jr} + N_i(b_{jr} + A_{jr} + Q_{jr}), \tag{15}$$

$$\frac{dN_m}{dt} = -N_2 b'_{jm} + N_i(b_{jm} + A_{jm} + Q_{jm}), \tag{16}$$

and,

$$\frac{dN_j}{dt} = N_r b'_{jr} + N_m b'_{jm} - N_j(b_{jr} + A_{jr} + Q_{jr} + b_{jm} + A_{jm} + Q_{jm}). \tag{17}$$

This system can be put in matrix form $\dot{\mathbf{X}} = \mathbf{A}\mathbf{X}$ as

$$\begin{bmatrix} \dot{N_r} \\ N_m \\ N_j \end{bmatrix} = \begin{bmatrix} -b'_{jr} & 0 & (b_{jr} + A_{jr} + Q_{jr}) \\ 0 & -b'_{jm} & (b_{jm} + A_{jm} + Q_{jm}) \\ b'_{jr} & b'_{jm} & -(b_{jr} + A_{jr} + Q_{jr} + b_{jm} + A_{jm} + Q_{jm}) \end{bmatrix} \begin{bmatrix} N_r \\ N_m \\ N_j \end{bmatrix} \tag{18}$$

This is a system of first order linear ODEs who's solutions is

$$\mathbf{X} = c_1\mathbf{E_1}e^{\lambda_1 t} + c_2\mathbf{E_2}e^{\lambda_2 t} + c_3\mathbf{E_3}e^{\lambda_3 t}. \tag{19}$$

Here, $\lambda_{1,2,3}$ are the eigenvalues of matrix $\mathbf{A}$, $E_{1,2,3}$ are the corresponding eigenvectors and $c_{1,2,3}$ are the constants of integration. The constants of integration are determined using the initial conditions at $t = 0$ (start of read pulse) which are $N_{r_0} = N_{j_0} = 0$, and $N_{m_0} = 1$, and in the second part of the model, the initial conditions are the populations at the end of the first part of the model; that is, Eqs. (19) are solved twice, once during the read-laser pulse, and once immediately following read-laser shutoff. The relevant values for the Einstein coefficients were found from the NIST lines database. The value for the re-excitation rate is calculated as $b'_{jm} = B'_{jm}I_\nu/c$, where I_ν is the incident laser intensity per unit frequency interval. The value of Q_{ji} was determined using the data presented in Hsu et al.,[52] and assumed to be the same for either excitation strategy as

$$Q_{ji} = P\left[X_{N_2}q_{N_2}\left(\frac{T}{294}\right)^{n_{N_2}} + X_{O_2}q_{O_2}\left(\frac{T}{294}\right)^{n_{O_2}} + X_{CO_2}q_{CO_2}\left(\frac{T}{294}\right)^{n_{CO_2}}\right]. \tag{20}$$

Here, X_{N_2}, X_{O_2}, and X_{CO_2} are the mole fractions of the species in the mixture, and q_{N_2}, q_{O_2}, q_{CO_2}, n_{N_2}, n_{O_2}, and n_{CO_2} are constants given in Hsu et al.[52] The values used in the model calculations are listed in Table 1.

Table 1: Transition Data. Note that j is the upper level, i is the lower level.

Transition (j-i)	Wavelength nm	A_{ji} s^{-1}	B_{ji} $\frac{m}{kg}$	B'_{ji} $\frac{m}{kg}$	$\frac{g_{ji}}{g_{ij}}$ -	b_{ji} s^{-1}	b'_{ji} s^{-1}
A $(e-m)$	760.15	3.1×10^{7}	8.17×10^{20}	8.17×10^{20}	1	3.8×10^{20}	3.8×10^{20}
B $(e-r)$	819.	1.1×10^{7}	3.6×10^{20}	6.05×10^{20}	$\frac{5}{3}$	0	0
C $(e'-m)$	769.45	5.6×10^{6}	1.53×10^{20}	9.18×10^{19}	$\frac{3}{5}$	7.21×10^{10}	4.33×10^{10}
D $(e'-r)$	829.81	3.2×10^{7}	1.09×10^{21}	1.09×10^{21}	1	0	0

The model developed above can be used to calculate the fluorescence signal resulting from a given gas mixture, thermodynamic state, read-laser pulse-intensity/duration, and re-excitation scheme. Fig. 9 illustrates the population dynamics of the old and the new re-excitation schemes. The re-excitation saturates quickly at 10^{-15} s in both cases. Note that the fluorescence is imaged only after the end of the read pulse by gating the camera. Also note that the $5s[3/2]_1$ level is more quickly populated with the new re-excitation scheme, which is an indicator of higher fluorescence.

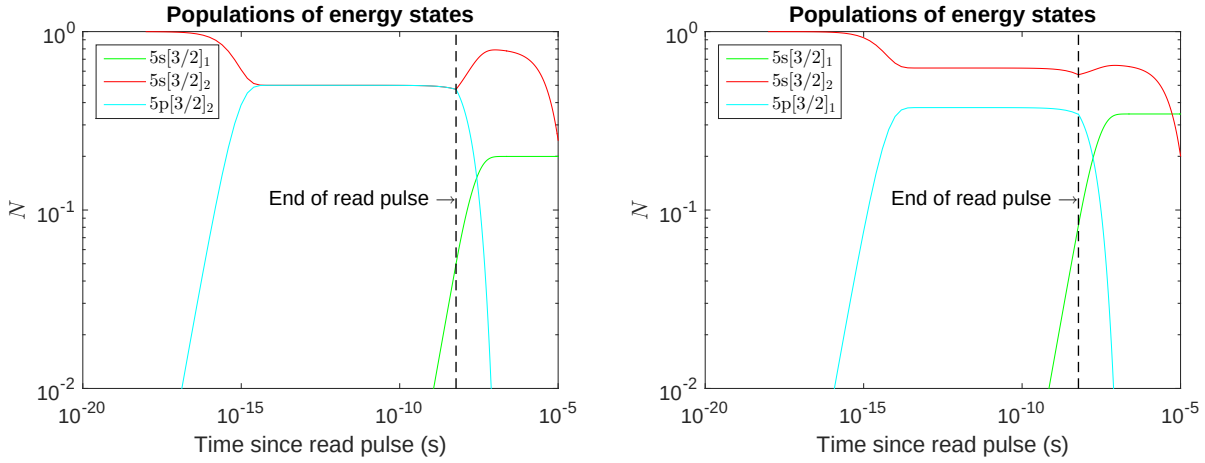

Figure 9: Populations of energy level with respect to time from beginning of read pulse. Note the saturation of the re-excitation transition. **Left:** Original re-excitation scheme. **Right:** Alternate re-excitationon scheme.

Fig. 10 (left) shows a plot of the fluorescence signal ($N_j A_{jr}$) from states e ($5p[3/2]_2$) and e' ($5p[3/2]_1$), which represent the anticipated fluorescence from the old and new re-excitation schemes, respectively. Note that the only difference is the re-excitation wavelength. The fluorescence imaged by the camera is proportional to the integral of $N_j A_{jr}$ from the the end of the read pulse. The ratio of the fluorescence from the alternative scheme to the original scheme, FSR, is

$$FSR = \frac{\int_{t_0}^{t_0+50\ ns} N_{e'} A_{e'r} dt}{\int_{t_0}^{t_0+50\ ns} N_e A_{er} dt}. \tag{21}$$

The value of this integral as evaluated in MATLAB using the solution of the system of ODEs given in Eq. (18) is shown in Fig. 10 (right) for a 99% N_2 and 1% Kr mixture. These properties are representative of the conditions in the tube during the experiments. The result indicates that the fluorescence from state e' to state r (new re-excitation scheme) is approximately twice as large as the fluorescence from state e to state r (old re-excitation scheme); thus, the alternative excitation scheme is advantageous because of higher SNR. Moreover, the switch in re-excitation schemes required no addition equipment changes other than the read-laser wavelength (old: 760.2 nm to new: 769.5 nm).

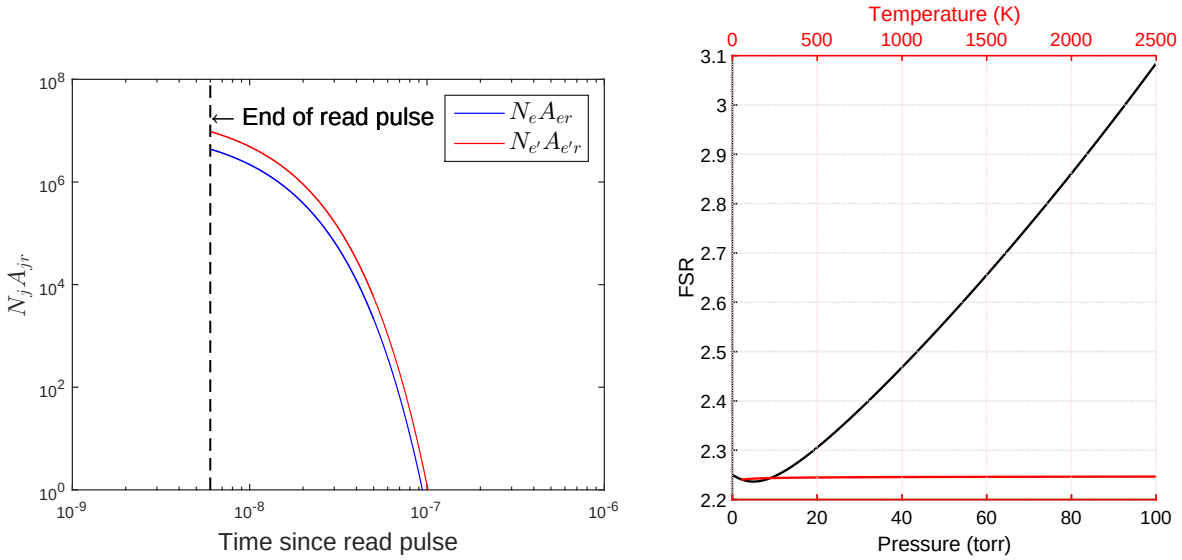

Figure 10: **Left:** Fluorescence comparison of the new and old re-excitation schemes. **Right:** FSR ratio vs. pressure (temperature fixed at 750 K) and FSR ratio vs. temperature (pressure fixed at 1 torr).

VII. Results

The freestream velocity behind the shock was measured with the KTV technique. All experiments were performed using a mixture of 99% N_2 and 1% Kr. This mixture was seeded into the shock tube via the intake port (see Fig. 1) from pre-mixed K-bottles. The pressure was maintained by simultaneously seeding the mixture into the tube and running the vacuum pumps. After the desired pressure was achieved, the diaphragm was ruptured and then the write and read locations were imaged with the camera. Three KTV lines were written with approximately 0.5 mJ/pulse each and the read-laser wavelength was 769.5 nm, with the rest of the setup similar to that in recent KTV work.[49]

During the experiment it was observed that the splitter plate was misaligned in pitch; unfortunately, nothing could be done to fix this as of this writing. To calculate u_{2LF} (for comparison with KTV results), it was assumed that the misalignment accelerated the flow via a Prandlt-Meyer expansion fan, as shown in Fig. 11.

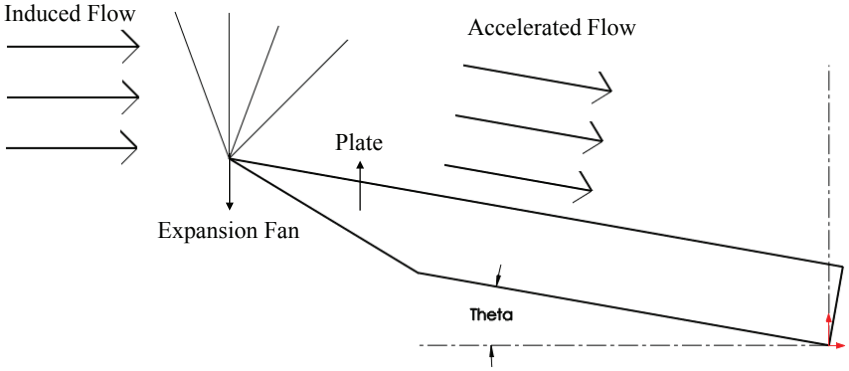

Figure 11: Acceleration of flow due to plate misalignment.

A value of 5 degrees was determined by measurement for the misalignment angle; so, a range of values for u_{2LF} was calculated assuming the flow was expanded by up to 5 degrees. The conditions of the two shots carried out (shot 50 and shot 51), along with the values of u_{2LF}, T_{2F}, and τ_F calculated using M_s, and the value of u_{2L} measured from KTV are presented in Table 2.

Table 2: Conditions and results of shots 50 and 51.

Shot	P_1	P_2	M_s	T_{2F}	τ_F	u_{2LF}	u_{2L}
	(Measured)	(Measured)	(Measured)	(Calc from M_s)	(Calc from M_s)	(Calc from M_s)	(Measured from KTV)
(#)	(Torr)	(Torr)	(-)	(K)	(s)	(m/s)	(m/s)
50	1.3	12.55	2.86	750	36.33	740-820	700-850
51	0.95	9.95	2.94	780	35.78	760-840	800-910

The KTV images for shots 50 and 51 are shown in Fig. 12 and Fig. 13. The image on the left is immediately after the write pulse, the image in the center is immediately after the read pulse, and the figure on the right shows the velocity results. The KTV velocity profiles are shown in black and the range of values of u_{2LF} is shown in red, as calculated from the shock speed measurement and the Prandtl-Meyer expansion. In each KTV exposure, three KTV lines were written and read 1.1 µs apart.

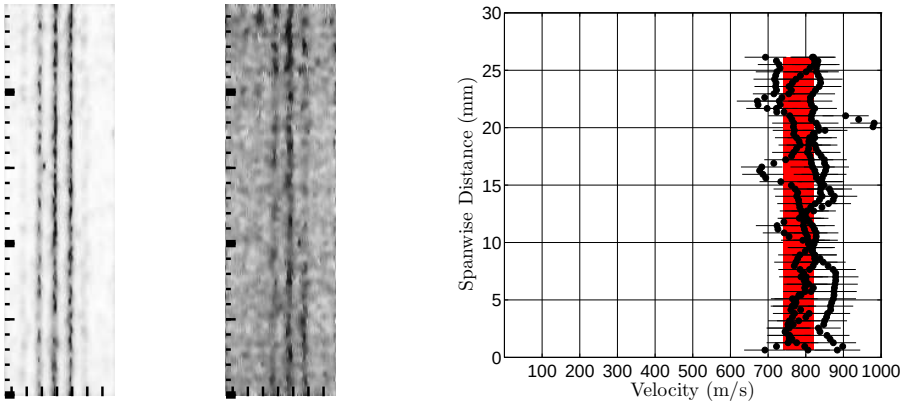

Figure 12: Shot 50 KTV results. **Left:** Exposure of three KTV lines after write pulse. Tick marks are millimeters. Inverse intensity scale. **Center:** Exposure of three KTV lines after read pulse. Tick marks are millimeters. Inverse intensity scale. **Right:** Velocity distribution. Black dots indicate KTV data. Horizontal bars indicate uncertainty in the KTV data. Red region depicts range of u_{2LF} values as calculated from the shock speed measurement and the Prandtl-Meyer expansion.

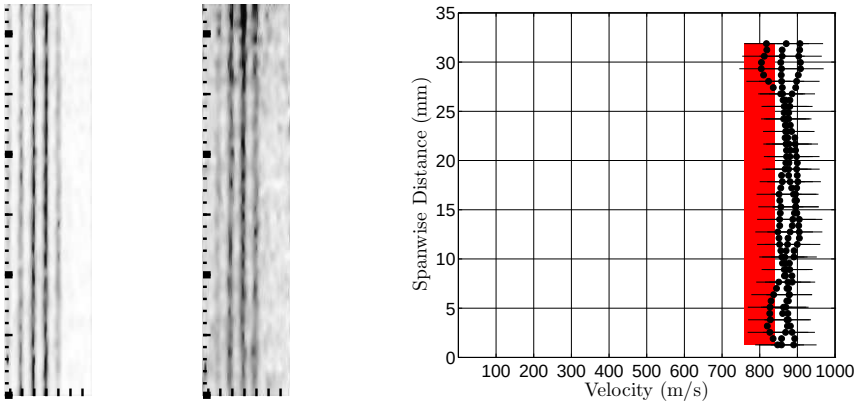

Figure 13: Shot 51 KTV results. **Left:** Exposure of three KTV lines after write pulse. Tick marks are millimeters. Inverse intensity scale. **Center:** Exposure of three KTV lines after read pulse. Tick marks are millimeters. Inverse intensity scale. **Right:** Velocity distribution. Black dots indicate KTV data. Horizontal bars indicate uncertainty in the KTV data. Red region depicts range of u_{2LF} values as calculated from the shock speed measurement and the Prandtl-Meyer expansion.

Shot 50 was the first experiment to show success, though the SNR is low. This was due to a complication with the write laser (old dye). For shot 51, the results appear more promising, although, this was the last

experiment performed before the solenoid that punctures the diaphragm failed. Regardless, shot 51 shows that KTV can likely be used in an impulse facility.

VIII. Conclusion

With the long-term goal of showing that KTV may be used in a large-scale impulse facility, we intended to sweep a parameter space by measuring profiles of velocity on a flat plate behind the incident shock in the Stevens Shock Tube. Although this goal was not achieved due to the failure of the rupturing mechanism during our testing period, promising data was recorded for several shots, two of which were described in this paper. Of particular note is that KTV was used for the first time at elevated temperature. As calculated from the shock-speed measurements, the temperature was in the range of 750-800 K.

In addition to the KTV results, we presented and justified a new re-excitation scheme for KTV which required no addition equipment, yet increased the SNR by a factor of approximately 2. This model will need further verification with experimental data. This verification data can be had from future experimental work with an underexpanded jet and the Stevens Shock Tube.

Acknowledgments

Mustafa and Parziale were supported by AFOSR Young Investigator Program Grant FA9550-16-1-0262 and equipment for this work was supported AFOSR DURIP Grant FA9550-15-1-0325; Ivett Leyva of AFOSR is the Program Manager for both grants. The authors thank Eric Marineau and Mike Smith of AEDC White Oak for their valuable insight and assistance. Also, the authors acknowledge the machine work done on the Stevens Shock Tube by Milan Simonovic, Marshall Reid, and George Wohlrab.

References

[1]Tropea, C., Yarin, A. L., and Foss, J. F., *Springer Handbook of Experimental Fluid Mechanics*, Springer, 2007.

[2]Haertig, J., Havermann, M., Rey, C., and George, A., "Particle Image Velocimetry in Mach 3.5 and 4.5 Shock-Tunnel Flows," *AIAA Journal*, Vol. 40, No. 6, 2002, pp. 1056–1060. doi: 10.2514/2.1787.

[3]Wagner, J. L., Beresh, S. J., DeMauro, E. P., Casper, K. M., Guildenbecher, D. R., Pruett, B. O., and Farias, P., "Pulse-Burst PIV Measurements of Transient Phenomena in a Shock Tube," *Proceedings of 54th AIAA Aerospace Sciences Meeting*, AIAA-2016-0791, San Diego, California, 2016. doi: 10.2514/6.2016-0791.

[4]Loth, E., "Compressibility and Rarefaction Effects on Drag of a Spherical Particle," *AIAA Journal*, Vol. 46, No. 9, 2008, pp. 2219–2228. doi: 10.2514/1.28943.

[5]Koochesfahani, M. M. and Nocera, D. G., "Molecular Tagging Velocimetry," *Springer Handbook of Experimental Fluid Mechanics*, edited by Tropea, C. and Yarin, A. L. and Foss, J. F., Springer, 2007.

[6]Hsu, A. G., Srinivasan, R., Bowersox, R. D. W., and North, S. W., "Molecular Tagging Using Vibrationally Excited Nitric Oxide in an Underexpanded Jet Flowfield," *AIAA Journal*, Vol. 47, No. 11, 2009, pp. 2597–2604. doi: 10.2514/1.39998.

[7]Hsu, A. G., Srinivasan, R., Bowersox, R. D. W., and North, S. W., "Two-component molecular tagging velocimetry utilizing NO fluorescence lifetime and NO_2 photodissociation techniques in an underexpanded jet flowfield," *Applied Optics*, Vol. 48, No. 22, 2009, pp. 4414–4423. doi: 10.1364/AO.48.004414.

[8]Sánchez-González, R., Srinivasan, R., Bowersox, R. D. W., and North, S. W., "Simultaneous velocity and temperature measurements in gaseous flow fields using the VENOM technique," *Optics Letters*, Vol. 36, No. 2, 2011, pp. 196–198. doi: 10.1364/OL.36.000196.

[9]Sánchez-González, R., Bowersox, R. D. W., and North, S. W., "Simultaneous velocity and temperature measurements in gaseous flowfields using the vibrationally excited nitric oxide monitoring technique: a comprehensive study," *Applied Optics*, Vol. 51, No. 9, 2012, pp. 1216–1228. doi: 10.1364/AO.51.001216.

[10]Sánchez-González, R., Bowersox, R. D. W., and North, S. W., "Vibrationally excited NO tagging by NO($A^2\Sigma^+$) fluorescence and quenching for simultaneous velocimetry and thermometry in gaseous flows," *Optics Letters*, Vol. 39, No. 9, 2014, pp. 2771–2774. doi: 10.1364/OL.39.002771.

[11]Dam, N., Klein-Douwel, R. J. H., Sijtsema, N. M., and ter Meulen, J. J., "Nitric oxide flow tagging in unseeded air," *Optics Letters*, Vol. 26, No. 1, 2001, pp. 36–38. doi: 10.1364/OL.26.000036.

[12]Sijtsema, N. M., Dam, N. J., Klein-Douwel, R. J. H., and ter Meulen, J. J., "Air Photolysis and Recombination Tracking: A New Molecular Tagging Velocimetry Scheme," *AIAA Journal*, Vol. 40, No. 6, 2002, pp. 1061–1064. doi: 10.2514/2.1788.

[13]Van der Laan, W. P. N., Tolboom, R. A. L., Dam, N. J., and ter Meulen, J. J., "Molecular tagging velocimetry in the wake of an object in supersonic flow," *Experiments in Fluids*, Vol. 34, No. 4, 2003, pp. 531–534. doi: 10.1007/s00348-003-0593-1.

[14]Miles, R., Cohen, C., Connors, J., Howard, P., Huang, S., Markovitz, E., and Russell, G., "Velocity measurements by vibrational tagging and fluorescent probing of oxygen," *Optics Letters*, Vol. 12, No. 11, 1987, pp. 861–863. doi: 10.1364/OL.12.000861.

[15]Miles, R., Connors, J., Markovitz, E., Howard, P., and Roth, G., "Instantaneous profiles and turbulence statistics of supersonic free shear layers by Raman excitation plus laser-induced electronic fluorescence (RELIEF) velocity tagging of oxygen," *Experiments in Fluids*, Vol. 8, No. 1-2, 1989, pp. 17–24. doi: 10.1007/BF00203060.

[16]Miles, R. B., Zhou, D., Zhang, B., and Lempert, W. R., "Fundamental Turbulence Measurements by RELIEF Flow Tagging," *AIAA Journal*, Vol. 31, No. 3, 1993, pp. 447–452. doi: 10.2514/3.11350.

[17]Miles, R. B. and Lempert, W. R., "Quantitative Flow Visualization in Unseeded Flows," *Annual Review of Fluid Mechanics*, Vol. 29, No. 1, 1997, pp. 285–326. doi: 10.1146/annurev.fluid.29.1.285.

[18]Miles, R. B., Grinstead, J., Kohl, R. H., and Diskin, G., "The RELIEF flow tagging technique and its application in engine testing facilities and for helium-air mixing studies," *Measurement Science and Technology*, Vol. 11, No. 9, 2000, pp. 1272–1281. doi: 10.1088/0957-0233/11/9/304.

[19]Michael, J. B., Edwards, M. R., Dogariu, A., and Miles, R. B., "Femtosecond laser electronic excitation tagging for quantitative velocity imaging in air," *Applied Optics*, Vol. 50, No. 26, 2011, pp. 5158–5162. doi: 10.1364/AO.50.005158.

[20]Edwards, M. R., Dogariu, A., and Miles, R. B., "Simultaneous Temperature and Velocity Measurements in Air with Femtosecond Laser Tagging," *AIAA Journal*, Vol. 53, No. 8, 2015, pp. 2280–2288. doi: 10.2514/1.J053685.

[21]Jiang, N., Halls, B. R., Stauffer, H. U., Danehy, P. M., Gord, J. R., and Roy, S., "Selective two-photon absorptive resonance femtosecond-laser electronic-excitation tagging velocimetry," *Optics Letters*, Vol. 41, No. 10, 2016, pp. 2225–2228. doi: 10.1364/OL.41.002225.

[22]Jiang, N., Mance, J. G., Slipchenko, M. N., Felver, J. J., Stauffer, H. U., Yi, T., Danehy, P. M., and Roy, S., "Seedless velocimetry at 100 kHz with picosecond-laser electronic-excitation tagging," *Optics Letters*, Vol. 42, No. 2, 2017, pp. 239–242. doi: 10.1364/OL.42.000239.

[23]Mills, J. L., *Investigation of Multi-Photon Excitation in Argon with Applications in Hypersonic Flow Diagnostics*, Ph.D. thesis, Old Dominion University, 2016.

[24]McDaniel, J. C., Hiller, B., and Hanson, R. K., "Simultaneous multiple-point velocity measurements using laser-induced iodine fluorescence," *Optics Letters*, Vol. 8, No. 1, 1983, pp. 51–53. doi: 10.1364/OL.8.000051.

[25]Balla, R. J., "Iodine Tagging Velocimetry in a Mach 10 Wake," *AIAA Journal*, Vol. 51, No. 7, 2013, pp. 1–3. doi: 10.2514/1.J052416.

[26]Barker, P., Bishop, A., and Rubinsztein-Dunlop, H., "Supersonic velocimetry in a shock tube using laser enhanced ionisation and planar laser induced fluorescence," *Applied Physics B*, Vol. 64, No. 3, 1997, pp. 369–376. doi: 10.1007/s003400050186.

[27]Lempert, W. R., Jiang, N., Sethuram, S., and Samimy, M., "Molecular Tagging Velocimetry Measurements in Supersonic Microjets," *AIAA Journal*, Vol. 40, No. 6, 2002, pp. 1065–1070. doi: 10.2514/2.1789.

[28]Lempert, W. R., Boehm, M., Jiang, N., Gimelshein, S., and Levin, D., "Comparison of molecular tagging velocimetry data and direct simulation Monte Carlo simulations in supersonic micro jet flows," *Experiments in Fluids*, Vol. 34, No. 3, 2003, pp. 403–411. doi: 10.1007/s00348-002-0576-7.

[29]Handa, T., Mii, K., Sakurai, T., Imamura, K., Mizuta, S., and Ando, Y., "Study on supersonic rectangular microjets using molecular tagging velocimetry," *Experiments in Fluids*, Vol. 55, No. 5, 2014, pp. 1–9. doi: 10.1007/s00348-014-1725-5.

[30]Boedeker, L. R., "Velocity measurement by H_2O photolysis and laser-induced fluorescence of OH," *Optics Letters*, Vol. 14, No. 10, 1989, pp. 473–475. doi: 10.1364/OL.14.000473.

[31]Wehrmeyer, J. A., Ribarov, L. A., Oguss, D. A., and Pitz, R. W., "Flame Flow Tagging Velocimetry with 193-nm H_2O Photodissociation," *Applied Optics*, Vol. 38, No. 33, 1999, pp. 6912–6917. doi: 10.1364/AO.38.006912.

[32]Pitz, R. W., Lahr, M. D., Douglas, Z. W., Wehrmeyer, J. A., Hu, S., Carter, C. D., Hsu, K.-Y., Lum, C., and Koochesfahani, M. M., "Hydroxyl tagging velocimetry in a supersonic flow over a cavity," *Applied Optics*, Vol. 44, No. 31, 2005, pp. 6692–6700. doi: 10.1364/AO.44.006692.

[33]Hiller, B., Booman, R. A., Hassa, C., and Hanson, R. K., "Velocity visualization in gas flows using laser-induced phosphorescence of biacetyl," *Review of Scientific Instruments*, Vol. 55, No. 12, 1984, pp. 1964–1967. doi: 10.1063/1.1137687.

[34]Gendrich, C. P. and Koochesfahani, M. M., "A spatial correlation technique for estimating velocity fields using molecular tagging velocimetry (MTV)," *Experiments in Fluids*, Vol. 22, No. 1, 1996, pp. 67–77. doi: 10.1007/BF01893307.

[35]Gendrich, C. P., Koochesfahani, M. M., and Nocera, D. G., "Molecular tagging velocimetry and other novel applications of a new phosphorescent supramolecule," *Experiments in Fluids*, Vol. 23, No. 5, 1997, pp. 361–372. doi: 10.1007/s003480050123.

[36]Stier, B. and Koochesfahani, M. M., "Molecular tagging velocimetry (MTV) measurements in gas phase flows," *Experiments in Fluids*, Vol. 26, No. 4, 1999, pp. 297–304. doi: 10.1007/s003480050292.

[37]Ribarov, L. A., Wehrmeyer, J. A., Batliwala, F., Pitz, R. W., and DeBarber, P. A., "Ozone Tagging Velocimetry Using Narrowband Excimer Lasers," *AIAA Journal*, Vol. 37, No. 6, 1999, pp. 708–714. doi: 10.2514/2.799.

[38]Moffat, R. J., "Contributions to the Theory of Single-Sample Uncertainty Analysis," *Journal of Fluids Engineering*, Vol. 104, No. 2, 1982, pp. 250–258. doi: 10.1115/1.3241818.

[39]Anderson, J. D., *Hypersonic and High Temperature Gas Dynamics*, AIAA, 2nd ed., 2011.

[40]Millikan, R. C. and White, D. R., "Systematics of Vibrational Relaxation," *The Journal of Chemical Physics*, Vol. 39, No. 12, 1963, pp. 3209–3213. doi: 10.1063/1.1734182.

[41]Goodwin, D. G., "An Open-Source, Extensible Software Suite for CVD Process Simulation," *Proceedings of CVD XVI and EuroCVD Fourteen, M Allendorf, F Maury, and F Teyssandier (Eds.)*, 2003, pp. 155–162.

[42]Browne, S., Ziegler, J., and Shepherd, J. E., "Numerical Solution Methods for Shock and Detonation Jump Conditions," GALCIT - FM2006-006, 2006.

[43]Mills, J. L., Sukenik, C. I., and Balla, R. J., "Hypersonic Wake Diagnostics Using Laser Induced Fluorescence Techniques," *Proceedings of 42nd AIAA Plasmadynamics and Lasers Conference*, AIAA 2011-3459, Honolulu, Hawaii, 2011. doi: 10.2514/6.2011-3459.

[44]Balla, R. J. and Everhart, J. L., "Rayleigh Scattering Density Measurements, Cluster Theory, and Nucleation Calculations at Mach 10," *AIAA Journal*, Vol. 50, No. 3, 2012, pp. 698–707. doi: 10.2514/1.J051334.

[45]Parziale, N. J., Smith, M. S., and Marineau, E. C., "Krypton Tagging Velocimetry for Use in High-Speed Ground-Test Facilities," *Proceedings of AIAA SciTech 2015*, AIAA-2015-1484, Kissimmee, Florida, 2015. doi: 10.2514/6.2015-1484.

[46]Parziale, N. J., Smith, M. S., and Marineau, E. C., "Krypton tagging velocimetry of an underexpanded jet," *Applied Optics*, Vol. 54, No. 16, 2015, pp. 5094–5101. doi: 10.1364/AO.54.005094.

[47]Zahradka, D., Parziale, N. J., Smith, M. S., and Marineau, E. C., "Krypton Tagging Velocimetry (KTV) in Supersonic Turbulent Boundary Layers," *Proceedings of AIAA SciTech 2016*, AIAA-2016-1587, San Diego, California, 2016. doi: 10.2514/6.2016-1587.

[48]Zahradka, D., Parziale, N. J., Smith, M. S., and Marineau, E. C., "Krypton tagging velocimetry in a turbulent Mach 2.7 boundary layer," *Experiments in Fluids*, Vol. 57, No. 62, 2016. doi: 10.1007/s00348-016-2148-2.

[49]Mustafa, M. A., Hunt, M. B., Parziale, N. J., Smith, M. S., and Marineau, E. C., "Krypton Tagging Velocimetry (KTV) Investigation of Shock-Wave/Turbulent Boundary-Layer Interaction," *Proceedings of AIAA SciTech 2017*, AIAA-2017-0025, Grapevine, Texas, 2017. doi: 10.2514/6.2017-0025.

[50]Chang, R. S. F., Horiguchi, H., and Setser, D. W., "Radiative lifetimes and twobody collisional deactivation rate constants in argon for Kr($4p^5 5p$) and Kr($4p^5 5p$) states," *The Journal of Chemical Physics*, Vol. 73, No. 2, 1980, pp. 778–790. doi: 10.1063/1.440185.

[51]Eckbreth, A. C., *Laser Diagnostics for Combustion Temperature and Species*, Gordon and Breach Publications, 2nd ed., 1996.

[52]Hsu, A. G., Narayanaswamy, V., Clemens, N. T., and Frank, J. H., "Mixture fraction imaging in turbulent non-premixed flames with two-photon LIF of krypton," *Proceedings of the Combustion Institute*, Vol. 33, No. 1, 2011, pp. 759–766. doi: 10.1016/j.proci.2010.06.051.